Hindawi
International Journal of Antennas and Propagation
Volume 2021, Article ID 6623468, 15 pages
https://doi.org/10.1155/2021/6623468

Research Article

Single-Arm Archimedean Spiral Antenna with Broadband Circular Polarization

Qingyuan Fang[1,2] **Mengzhe Jin**[1] **and Weidong Liu**[1]

[1]*Hebei Key Laboratory for Electromagnetic Environmental Effects and Information Processing, Shijiazhuang Tiedao University, Shijiazhuang 050003, China*
[2]*National Key Laboratory on Electromagnetic Environment Effects, Shijiazhuang Campus, Army Engineering University of PLA, Shijiazhuang 050043, China*

Correspondence should be addressed to Weidong Liu; liuwd_83@163.com

Received 24 December 2020; Revised 24 May 2021; Accepted 15 June 2021; Published 28 June 2021

Academic Editor: Stefania Bonafoni

In this paper, a single-arm Archimedean spiral (SAAS) antenna with broadband circular polarization is investigated. Unlike traditional single-arm Archimedean spiral antenna, the antenna arm consists of a hybrid meandered strip line and a smooth arc strip line. Especially at low frequencies, the meandered strip line significantly improves the circular polarization performance by extending the antenna surface current path. The effects of the meandered strip line on the radiation pattern and axial ratio (AR) are studied in detail. To obtain unidirectional radiation, a metallic cavity is added below the SAAS antenna. The measurement results show that the voltage standing wave ratio (VSWR) is less than 2 from 0.88 GHz to 8.82 GHz, which indicates a wide impedance bandwidth of 1 : 10 is realized. A wide AR bandwidth of 1 : 5 is available, that the measured AR is less than 3 dB from 1.6 GHz to 8 GHz.

1. Introduction

Pantograph arcing, caused by the separation of the pantograph and the contact wire, is very common in high-speed railways. Pantograph arcing can generate wideband electromagnetic interferences, which are mostly random and varies with frequency. Circularly polarized (CP) antennas [1–3], which are extensively applied in satellite communication systems, can be applied to pantograph arcing detection. Among circularly polarized antennas, Archimedean spiral antennas have attracted extensive attention because of their broad bandwidth, stable half power beam width (HPBW), and good circular polarization (CP) properties [4–7]. A traditional Archimedean spiral antenna has two symmetrical arms and requires balanced excitations, which limits its applications in engineering applications. A single-arm Archimedean spiral antenna, which takes one-half the space of a traditional Archimedean spiral antenna and does not need balanced excitations, is preferred in UWB communication applications because of its compact size [8–10].

A two-arm Archimedean spiral antenna is excited in an unbalanced mode [11]. This unbalanced mode spiral antenna does not need balanced excitation and exhibits good CP properties. It turns out that an unbalanced mode can be applied in spiral antenna design. In [12], the performance of a single-arm spiral antenna reveals that wide bandwidth and a good axial ratio over a wide frequency band are possible. The relationship between the radiation patterns and arm length for a single-arm rectangular spiral antenna is extensively studied in [13]. A conical-disc-backed single-arm Archimedean spiral antenna is designed to cover the X-band from 8 to 12 GHz [9]. A single-arm hexagonal spiral antenna array having a 30° beam scan without a grating lobe can operate from 2 to 6 GHz [14]. The method of moments (MOM) is applied to analyze the impedance and radiation pattern of the single-arm spiral antenna excited via a vertical probe [15]. The calculated results show that the single-arm spiral antenna has a wide impedance bandwidth and good circular polarization performance over a wide range of arm lengths (from $3.3\lambda_0$ to $4.9\lambda_0$, where λ_0 is the wavelength of

the central frequency). The conformal finite difference time domain (FDTD) method is applied in analyzing the performance of the microstrip muscle-loaded single-arm Archimedean spiral antenna [16]. The abovementioned numerical calculation results provide that the single-arm spiral antenna has broad bandwidth and good CP performance. A wideband antenna array consisting of single-arm spiral antennas is designed in [17]. An excellent AR of less than 0.74 dB is realized by rotating each single-arm spiral antenna sequentially together while imposing a proper phase shift. The research results from [18] demonstrate that the radiating direction of a single-arm spiral antenna depends on the arm length. A tilted-beam spiral antenna with a single-arm is used in a multiband multipolarization shared-aperture antenna [8]. A single-arm rectangular spiral antenna that utilizes a set of microelectromechanical system (MEMS) switches to obtain a reconfigurable scan beam is discussed in [19]. An adaptive beam is realized by introducing variations in current distributions by using switches. A single-arm rectangular spiral antenna, which can realize reconfigurable radiation patterns, is realized by using four switches over a high-impedance surface [20]. The meandered line is demonstrated as an effective way to reduce the antenna size [21, 22]. A reflector plane with wideband balun instead of absorber and cavity is employed to realize a low-profile spiral antenna [23]. Coplanar waveguide transmission line fed spiral antenna without using an external balun or matching network is available to realize compact antenna structure [24]. Broadband circular polarization is an important aspect of the spiral antenna design. A circular reflector with one circular slot at the junction of two orthogonal rectangular slots is designed to improve the performance of AR [25]. The effect of the meandered line on the circular polarization performance has not been studied in single-arm spiral antenna design until now, so we will discuss the meandered line in improving the AR of the single-arm spiral antenna.

This paper presents a printed low-cost single-arm Archimedean spiral (SAAS) antenna. The antenna arm employs a meandered strip line to enhance the circular polarization performance at low frequencies. The meandered strip line SAAS antenna is studied and compared with a classical SAAS antenna to demonstrate its good circular polarization performance. Simulation results show that the AR of the proposed SAAS antenna is lower than that of the classical SAAS antenna. The meandered strip line effectively extends the antenna surface current path that improves the AR of the classical SAAS antenna. Moreover, a metallic cavity is employed to transform the bidirectional beam into the unidirectional beam. The simulated and measured results indicate that the proposed SAAS antenna with a metallic cavity has a wide impedance bandwidth and AR bandwidth.

2. Antenna Design and Configuration

Figure 1 shows the configuration of the proposed SAAS antenna. As shown in Figure 1(a), the SAAS antenna is composed of a single-arm, a substrate, a conducting disc ground (acting as the ground plane) and a coaxial feeding probe. The SAAS antenna arm is defined by the Archimedean function $r = a\varphi$, where $a = 0.75$ mm/rad is the spiral constant and φ is the winding angle. Unlike classical single-arm spiral antenna, this SAAS antenna arm exploits a hybrid strip line rather than a smooth arc line [12]. A smooth arc strip line and a meandered strip line are employed in the inner loops and outer loops, respectively. They are directly connected together at point A, as shown in Figure 1(c). Because the meandered strip line is helpful in extending the current path, it is used to improve the antenna circular polarization performance at low frequencies. The effects of the meandered strip line on the antenna performance are studied in the following section.

Traditional spiral antennas with two spiral arms need balanced excitations. A balun is needed to provide balanced excitations [22]. Benefiting from the unbalanced structure, the SAAS antenna can be excited by unbalanced feeding, e.g., a coaxial probe, as shown in Figure 1(a). As shown in Figure 1(b), the outer conductor and inner conductor of the coaxial probe are connected to the disc ground (radius $r_g = 25$ mm) and the antenna arm, respectively. Without balun, the SAAS antenna gets a compact structure via unbalanced feeding. An FR4 substrate, whose dielectric constant is 4.2, thickness $h = 2$ mm, and radius $r_s = 68$ mm, is exploited in the SAAS antenna. The detailed SAAS antenna arm configuration is exhibited in Figure 1(c). The smooth arc strip line (width $w_a = 2.4$ mm) moves around the z-axis from point O ($\varphi_s = 0.5\pi$) to point A ($\varphi_e = 13.5\pi$). Then, the meandered strip line (width $w_m = 3.0$ mm) is applied to the rest of the outer loops. The meandered strip line starts from point A ($\varphi_e = 13.5\pi$) to point B ($\varphi_m = 27\pi$). All the parameters are obtained through antenna optimization.

3. Results and Discussion

3.1. Comparisons between Antennas Using Meandered Strip Line and Smooth Arc Strip Line. Two Archimedean spiral antennas are simulated, as shown in Figure 2. In Figure 2(a), the winding angles are $\varphi_s = 0.5\pi$, $\varphi_e = 13.5\pi$ and $\varphi_m = 27\pi$. In Figure 2(b), the winding angles are $\varphi_s = 0.5\pi$ and $\varphi_m = 27\pi$.

The simulated reflection coefficient of both antennas is illustrated in Figure 3. It is noticed in Figure 3 that the proposed SAAS antenna has a lower reflection coefficient (0.24 GHz to 0.76 GHz) at low frequencies. Because the electrical current flowing along the antenna arm is extended on the meandered strip line. Generally, the lowest working frequency of a traditional Archimedean antenna with two arms can be estimated by $2\pi r \approx \lambda_L$ (r is the radius of the Archimedean antenna and λ_L is the wavelength of the lowest working frequency). This approach is also applicable for a single-arm Archimedean antenna [12]. However, exactly one wavelength is not adequate to obtain a good refection coefficient at the lowest working frequency. The circumference is chosen to be approximately two wavelengths at the lowest frequency [11]. For this SAAS antenna, compact size is expectable. Notice that in Figure 3, the reflection coefficient is less than −10 dB from 0.7 GHz. The radius of antenna r_s is

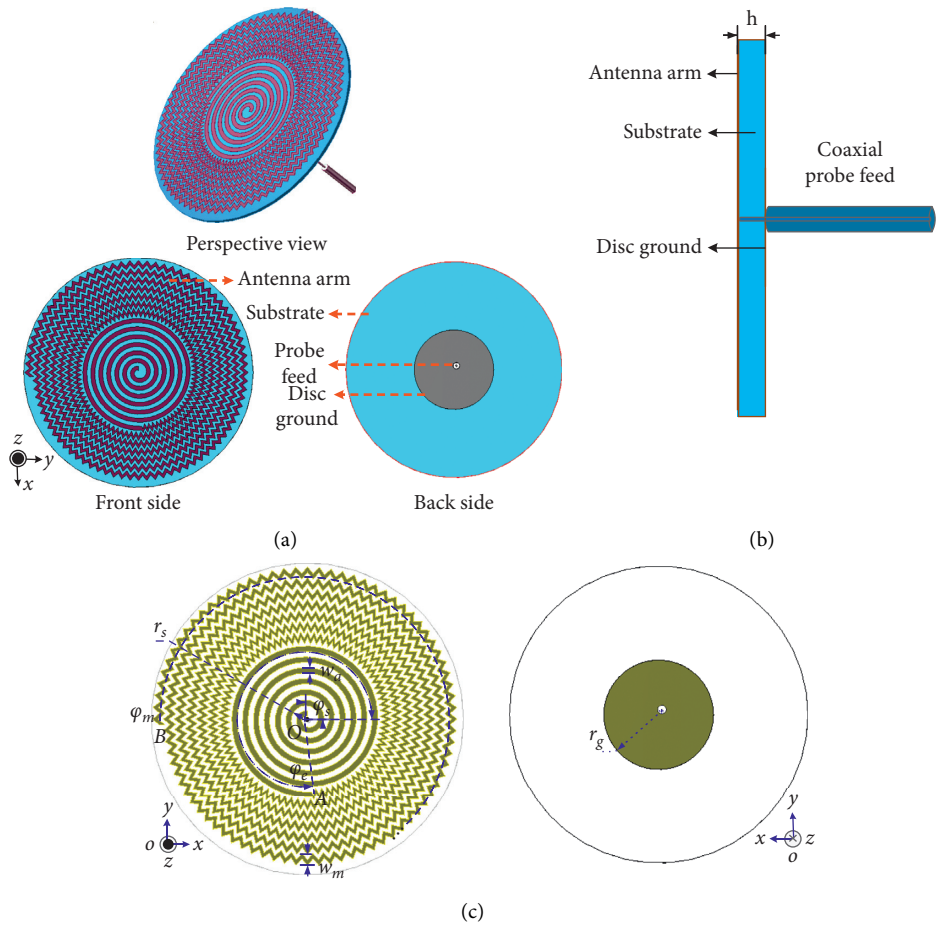

Figure 1: The SAAS antenna configuration. (a) Perspective view. (b) Side view. (c) Front view and back view.

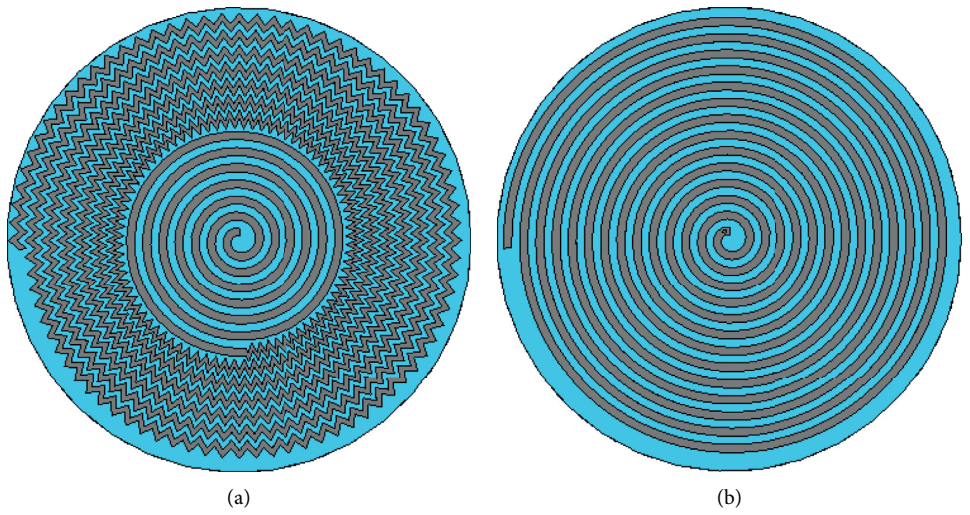

Figure 2: Simulated antenna models. (a) The proposed SAAS antenna. (b) The classical SAAS antenna.

68 mm, and the circumference is exactly one wavelength of the lowest working frequency, 0.7 GHz.

The axial ratios (ARs) at 0.8 GHz and 1 GHz for both antennas are shown in Figure 4. As shown in Figure 4(a), the AR of the classical SAAS antenna exceeds 3 dB at 0.8 GHz, so the circular polarization is not well performed. The AR of the proposed SAAS antenna is less than 3 dB from −50° to 50°, and its minimum is less than 1 dB. This result means that

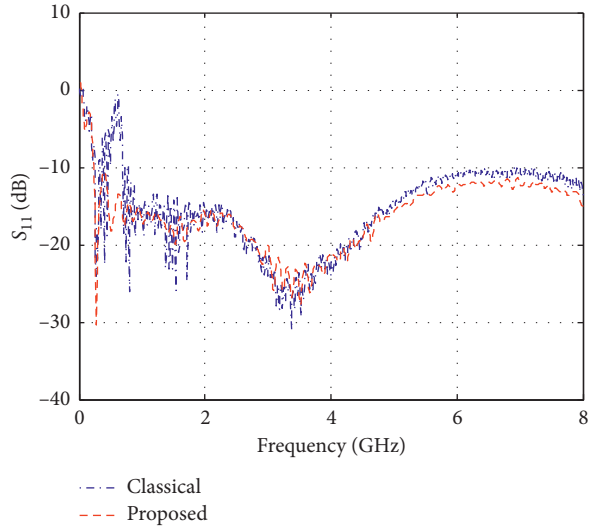

Figure 3: Simulated reflection coefficient of antennas with different arm shapes.

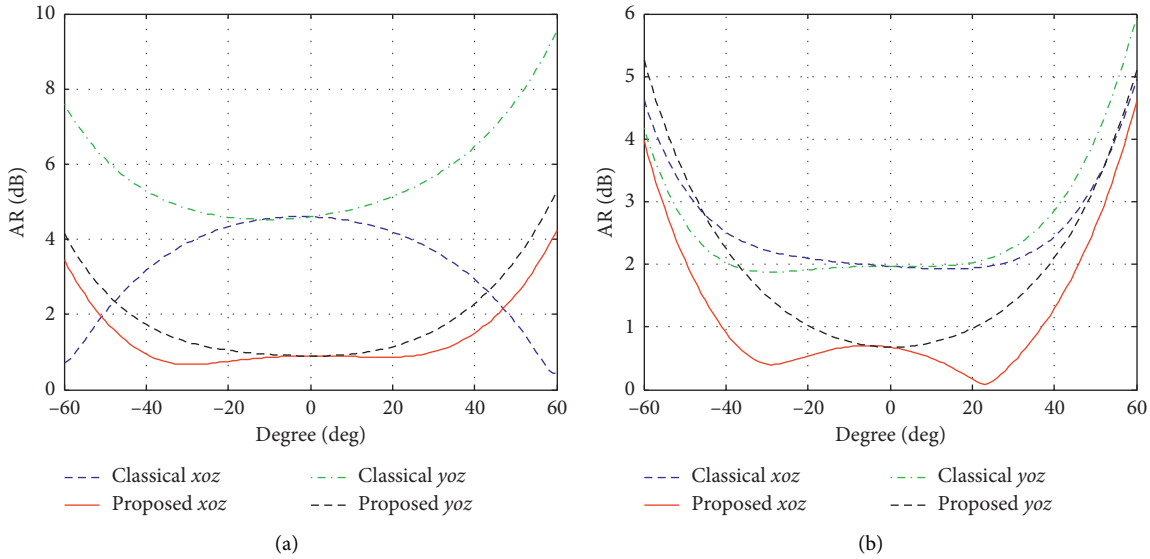

Figure 4: Simulated axial ratio. (a) 0.8 GHz. (b) 1 GHz.

good circular polarization is available. Similarly, as can be observed from Figure 4(b), good CP is realized at 1 GHz for the proposed SAAS antenna. The AR is within 3 dB from −40° to 40°, which is lower than that of the classical SAAS antenna.

The AR improvement of the proposed SAAS antenna can be explained by the behavior of the surface current along the antenna arms. We draw a spiral line along the center of the antenna arm. Then the current data can be derived from the current simulation, which is described in Figure 5. Figure 5 shows the absolute value of the surface current along the spiral line. At the end of the antenna arm, the current of the proposed SAAS antenna is much less than that of the classical antenna. This indicates that the meandered strip line can better attenuate the surface current. The current reflected from the end of the proposed SAAS antenna arm is reduced. The reflected current can deteriorate the AR, which is harmful to the circular polarization performance. Hence, we can infer that the meandered strip line is effective in improving the CP performance of the SAAS antenna.

The radiation patterns of both antennas at 0.8 GHz are shown in Figure 6. As observed from Figures 6(a) and 6(b), the proposed and the classical SAAS antennas show similar radiation performance. The difference between the antenna gains is less than 0.11 dB, and the difference between the 3 dB beam width is less than 6°, which means the proposed SAAS antenna has similar radiation patterns with the classical SAAS antenna, and stable half power beam width (HPBW) is available for the proposed SAAS antenna.

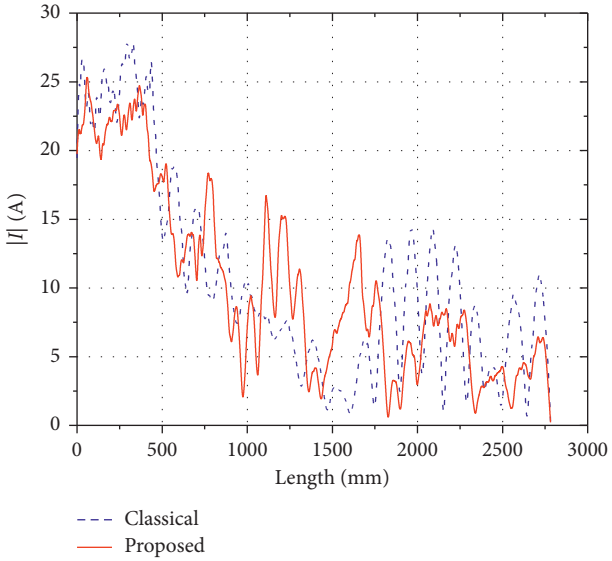

Figure 5: Current distribution along the antenna arms at 0.8 GHz.

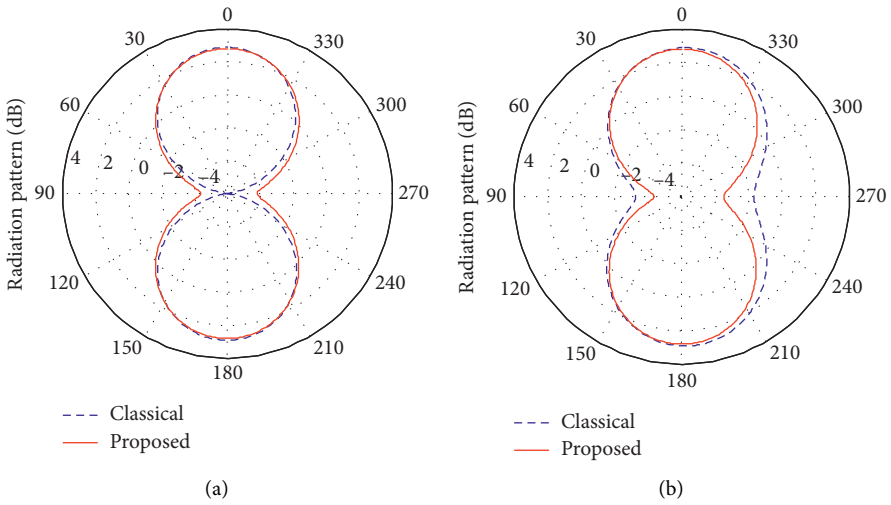

Figure 6: Simulated radiation patterns. (a) *xoz* plane at 0.8 GHz. (b) *yoz* plane at 0.8 GHz.

3.2. Study of Meandered Strip Line. It is illustrated in the above section that the SAAS antenna has better circular polarization using a hybrid strip line than a traditional smooth arc line. The parameter φ_e, which determines the position of the connection point A, will affect the circular polarization performance. The ARs of the SAAS antenna with different φ_e are shown in Figure 7. The AR is below 3 dB from -40° to 40° at 1 GHz when φ_e is 13.5π, which still holds as the frequency increasing to 6 GHz in *xoz* plane. The circular polarization at a lower frequency is the key factor that determines the configuration of the SAAS antenna. Thus, we set the connection point A at $\varphi_e = 13.5\pi$.

The width of the antenna arm is an important factor in antenna design. We study the influence of the parameter w_a on the antenna performance. The simulated reflection coefficient of the SAAS antenna with different w_a is shown in Figure 8. When the frequency is below 1 GHz, the S_{11} is better as w_a is 2.4 mm. The S_{11} is similar with different w_a when the frequency is higher than 5 GHz. Thus, we get that the influence of w_a on the S_{11} performance is not significant at higher frequencies. The minimum of S_{11} is between 2 GHz and 5 GHz, which shifts to a higher frequency as width increases. The simulated ARs of the SAAS antenna with different w_a at 1 GHz are shown in Figure 9. The AR is less than 2 dB from -49° to 46° in *xoz* plane when the w_a is 2.4 mm, which is better than others. It is less than 3 dB from -47° to 47° in *yoz* plane. The antenna can realize a better circular polarization when the width of the antenna arm is set to 2.4 mm.

The width of the meandered strip line w_m is also studied. The simulated reflection coefficient of the SAAS antenna with different w_m is shown in Figure 10. S_{11} is better as

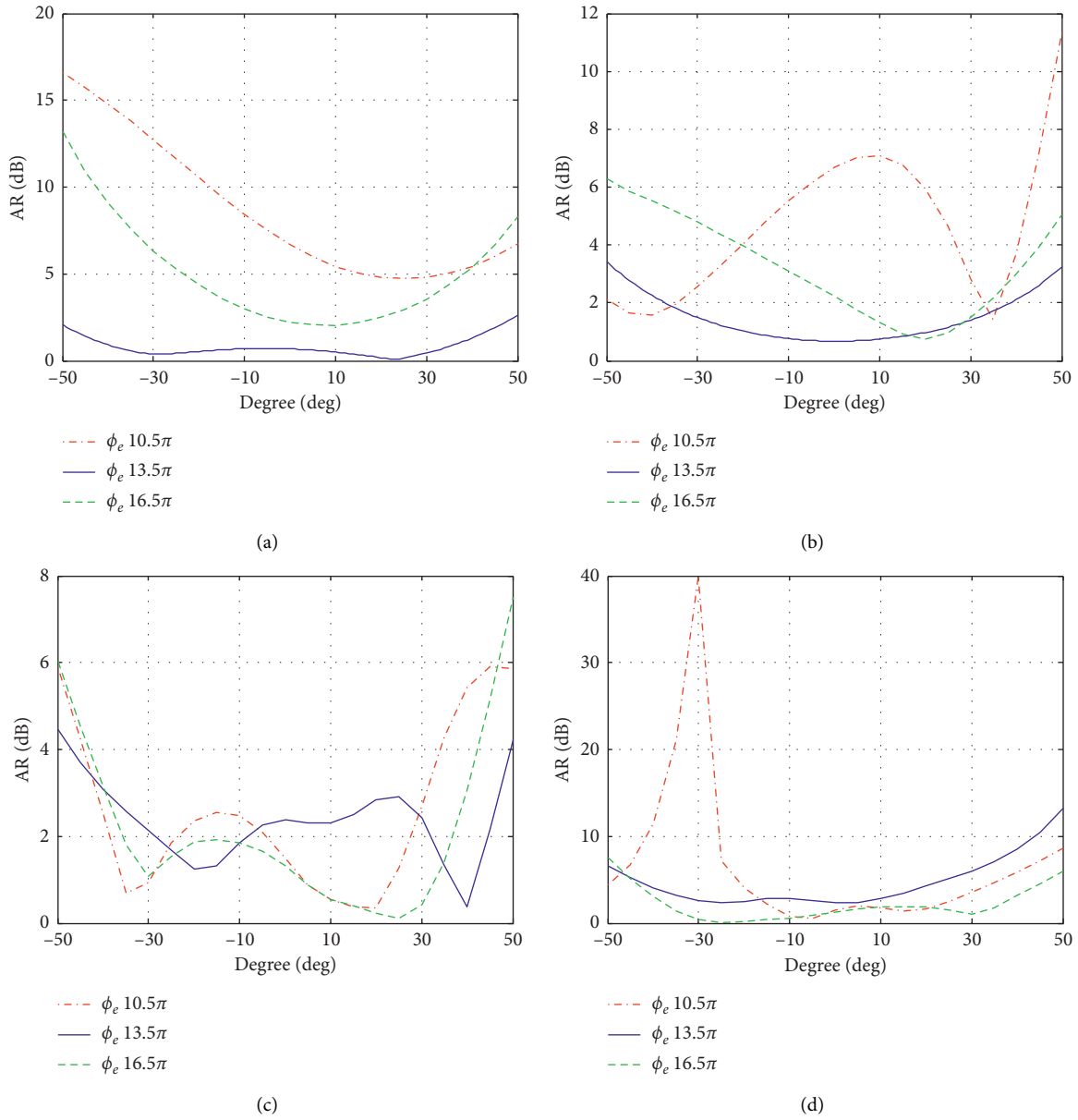

FIGURE 7: The simulated AR with different φ_e. (a) *xoz* plane at 1 GHz. (b) *yoz* plane at 1 GHz. (c) *xoz* plane at 6 GHz. (d) *yoz* plane at 6 GHz.

$w_m = 3.0$ mm when the frequency is below 1 GHz and higher than 5 GHz. The performance of S_{11} is similar between 2 GHz and 5 GHz with different w_m, while the minimum of S_{11} is different. The simulated ARs of the SAAS antenna with different w_m at 1 GHz are shown in Figure 11. As shown in Figure 11, the AR is less than 3 dB from -47° to 47° in both *xoz* and *yoz* planes when w_m is 3.0 mm, which is better than others. Thus, we set the value of w_m to 3.0 mm to get a better circular polarization at a lower frequency.

3.3. Study of Disc Ground. The disc ground, etched on the back side of the SAAS antenna, has a crucial influence on the reflection coefficient. Simulated results of the reflection coefficient with different disc ground radii are shown in Figure 12. Notice that the reflection coefficient deteriorates as the disc ground radius increases. Especially in a lower frequency band, the reflection coefficient with a radius of 5 mm is much worse than that with a radius of 25 mm.

The input impedance values of the proposed SAAS antennas with different disc radii are shown in Figure 13. The SAAS with a small disc ground (radius of 5 mm) has a small resistance from 0.23 GHz to 1 GHz, and its reactance fluctuates dramatically compared with the others. It follows that the disc ground has an intensive influence on the antenna performance in lower frequency band. Thus, the radius of the disc ground is set to 25 mm in the following simulations.

The simulated ARs at different frequencies for SAAS antennas with different disc ground radii are shown in Figure 14. As shown in Figure 14, the ARs exhibit similar trends. That is, the AR deteriorates as the frequency

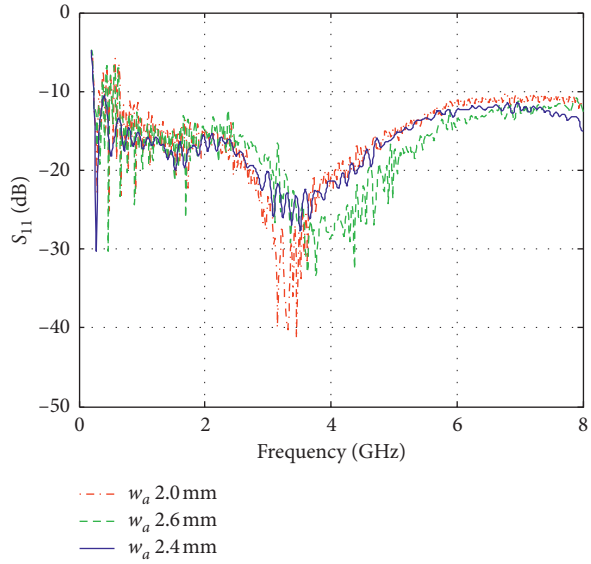

Figure 8: Simulated reflection coefficient of antennas with different w_a.

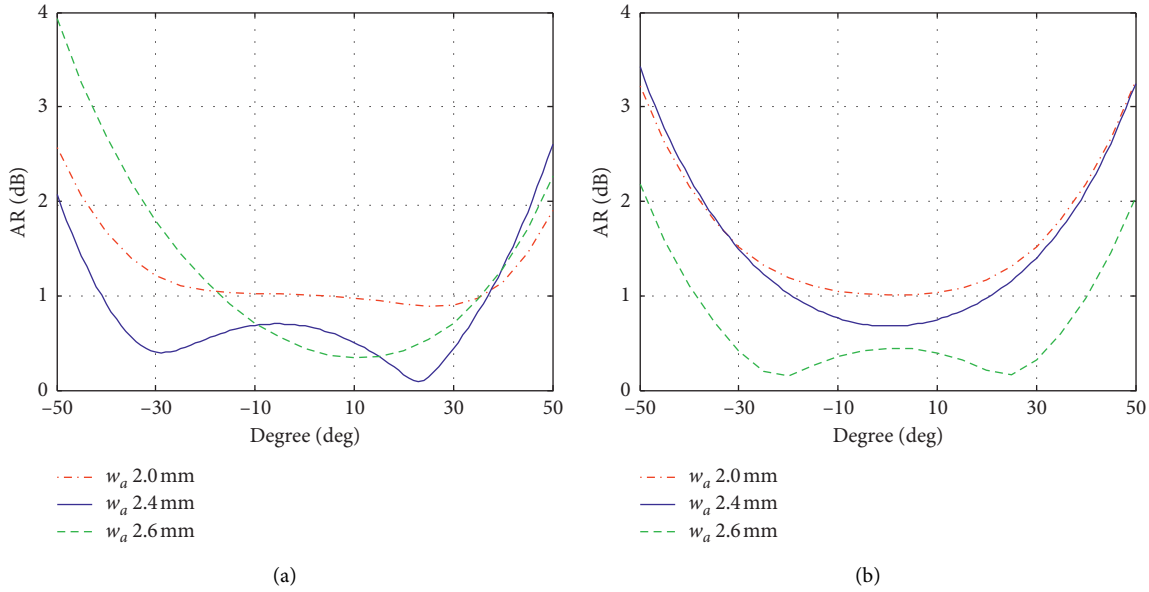

Figure 9: The simulated AR with different $w_a$at 1 GHz. (a) *xoz* plane. (b) *yoz* plane.

increases. Most of the ARs are less than 3 dB when the frequency is below 6 GHz. An antenna with a small disc ground (15 mm) has better performance when the frequency is below 5 GHz. This is because the disc ground act as a reflector will cause distortion of the current on the antenna arm, which degrades the AR performance. Thus, a small disc ground is preferred to get good circular polarization.

3.4. The SAAS Antenna with Metallic Back Cavity. To realize unidirectional radiation, the proposed SAAS antenna backed by a metallic cavity is simulated, as shown in Figure 15. The height of the metallic cavity is 100 mm, which is $0.26\lambda_L$ (λ_L is the lowest working frequency, 0.80 GHz). The metallic cavity is filled with absorbing material (dielectric constant 4.1, dielectric loss $\tan\delta = 0.7$) to improve the reflection coefficient in lower frequency band. The simulated reflection coefficient of the SAAS antenna with and without a cavity is illustrated in Figure 16. It can be observed from Figure 16 that the reflection coefficient of the SAAS antennas with and without a cavity has a similar performance.

The simulated ARs at different frequencies of the SAAS antenna with and without a cavity are shown in Figure 17. The AR of the SAAS antenna with a cavity is higher than 3 dB when the frequency is below 1.4 GHz, which is worse than that obtained without a cavity. The AR performance

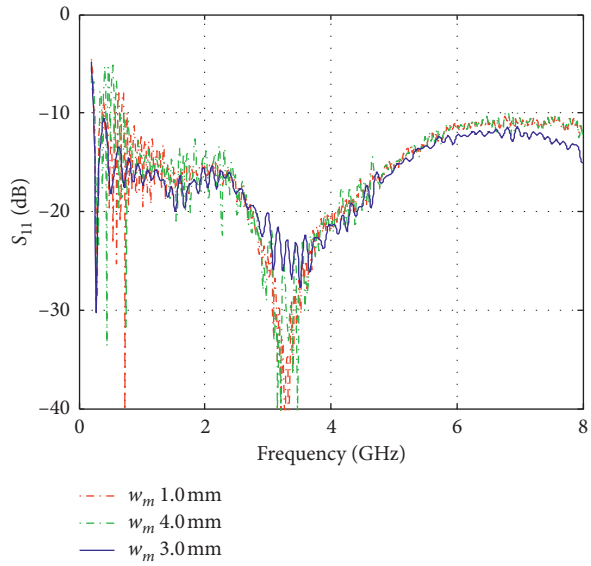

Figure 10: Simulated reflection coefficient of antennas with different w_m.

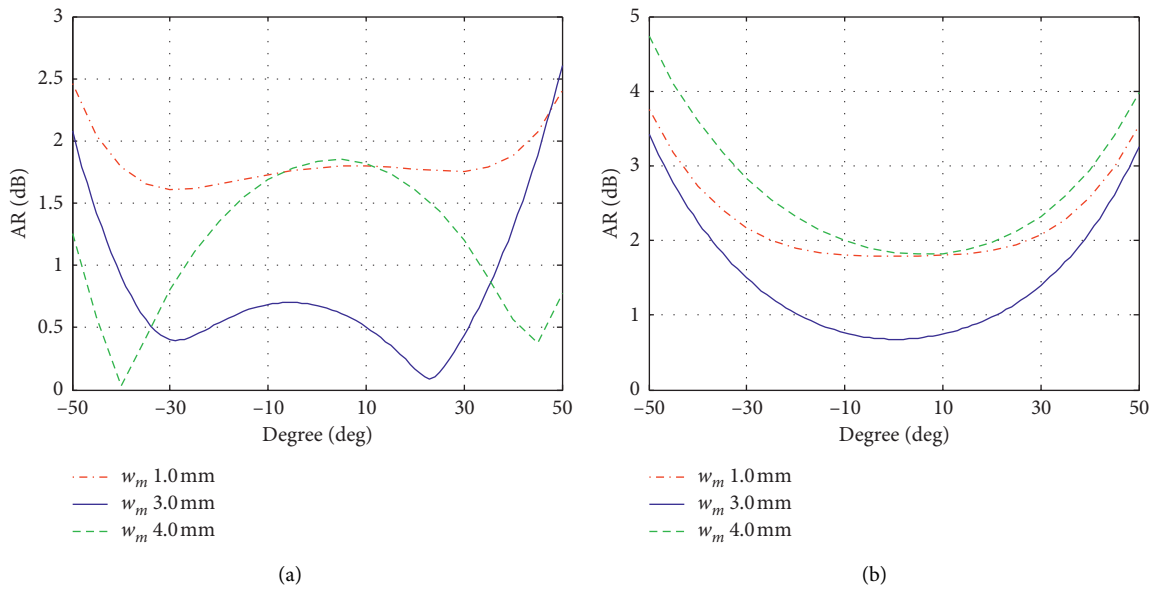

Figure 11: The simulated AR with different w_m at 1 GHz. (a) *xoz* plane. (b) *yoz* plane.

degradation in lower frequency is caused by the metallic cavity. The radiated electromagnetic waves from the antenna arm are reflected by the cavity, which can change the surface current distribution on the antenna arm, thus leading to AR degradation. The reflected electromagnetic waves cannot be completely absorbed in a wide frequency band. The wavelength of the lower frequency is longer. Thus the AR is more susceptible to be influenced by the cavity.

The simulated ARs at different frequencies of the SAAS antenna with different heights of the cavity are shown in Figure 18. The AR has a wider bandwidth when the height of the cavity is 100 mm compared with other values. That means a higher height of the cavity has less influence on the AR. As the height of the cavity increases, the AR becomes lower, and the circular polarization becomes better.

4. Experiment and Discussion

As shown in Figure 19, the SAAS antenna prototype with the parameters shown in Figure 1 is fabricated and measured with an Agilent E8363B vector network analyzer.

The simulated and measured results of the reflection coefficient S_{11} are presented in Figure 20. The measurement results of the antenna prototype show that the S_{11} is below −10 dB from 0.89 GHz to 8.58 GHz. Also, we can get that the voltage standing wave ratio (VSWR) is less than 2 from

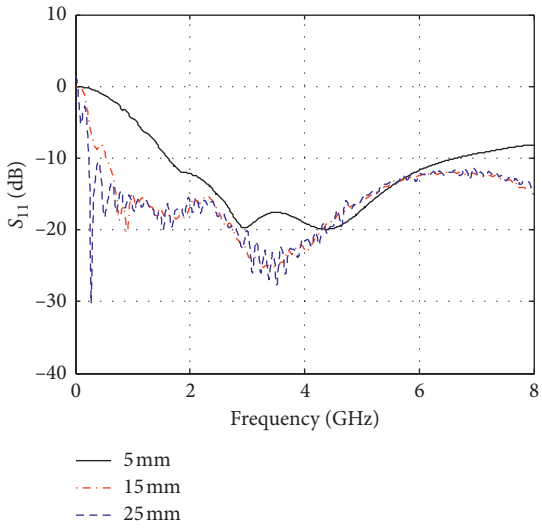

Figure 12: Simulated reflection coefficient of antennas with different disc ground radii.

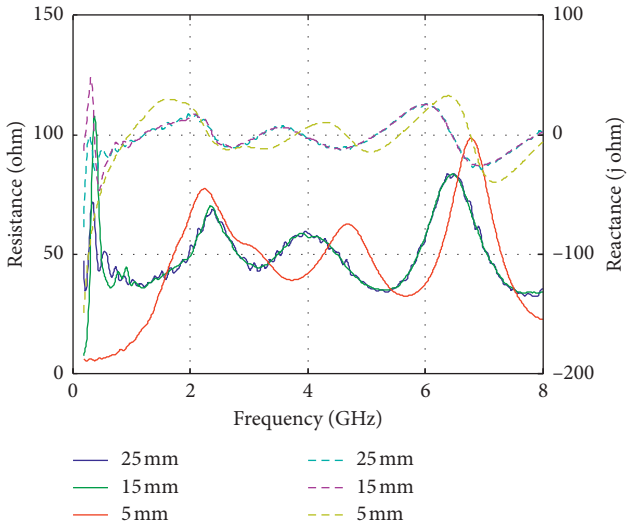

Figure 13: Simulated input impedance of antennas with different disc ground radii.

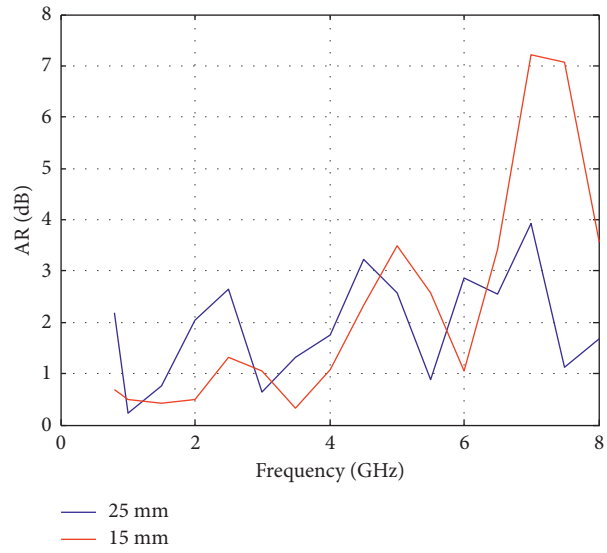

Figure 14: Simulated AR of antennas with different disc ground radii.

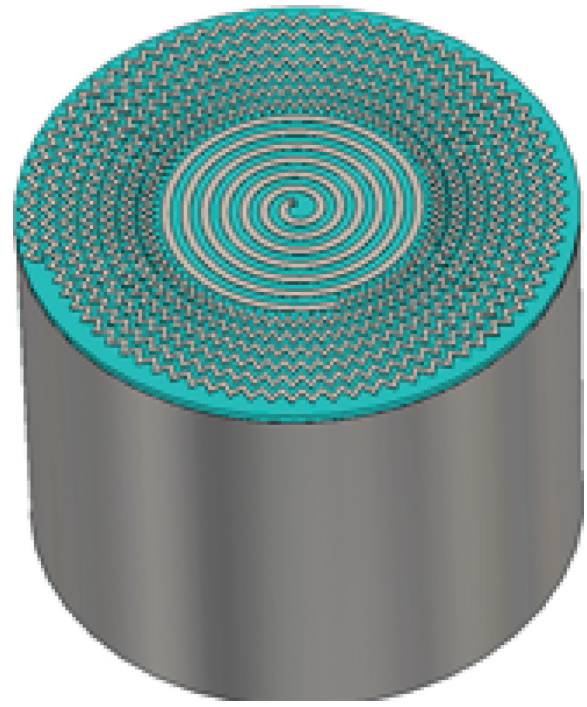

Figure 15: Simulated model of the SAAS antenna with a metallic cavity.

0.88 GHz to 8.82 GHz, which illustrates a bandwidth of 1 : 10. The difference between the measured and simulated results might be attributed to the following reasons. Firstly, to decrease the antenna model complexity and save the simulation time, the subminiature version A connector is replaced by an ideal port to feed the antenna in the simulation. It may cause undesirable reflection in the antenna prototype and lead to the difference between the measured and simulated results of S_{11}. Secondly, the antenna arms and the ground are set to be a perfect conductor in the simulation. They are made of copper and silver-plated, whose surface roughness can change the current distribution, which might lead to the current reflection. Thirdly, the inconsistency of the dielectric constant and the thickness of the substrate may cause the S_{11} degradation in the antenna prototype.

The SAAS antenna prototype shown in Figure 19 has bidirectional radiation. To realize unidirectional radiation, a metallic cavity filled with an absorber is employed, as shown in Figure 21. The height of the cavity is 100 mm, which is $0.29\lambda_L$ (λ_L is the lowest working frequency, 0.88 GHz). The VSWR of the SAAS antenna with a back cavity is exhibited in Figure 22. It is demonstrated that the cavity with an absorber

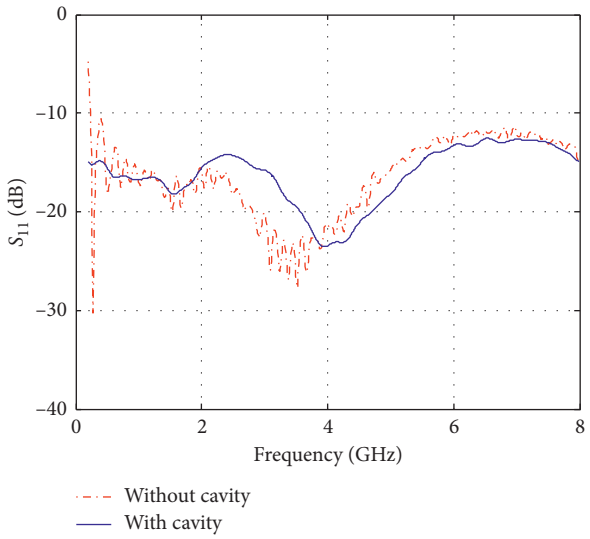

Figure 16: Simulated reflection coefficients of the SAAS antennas with and without a cavity.

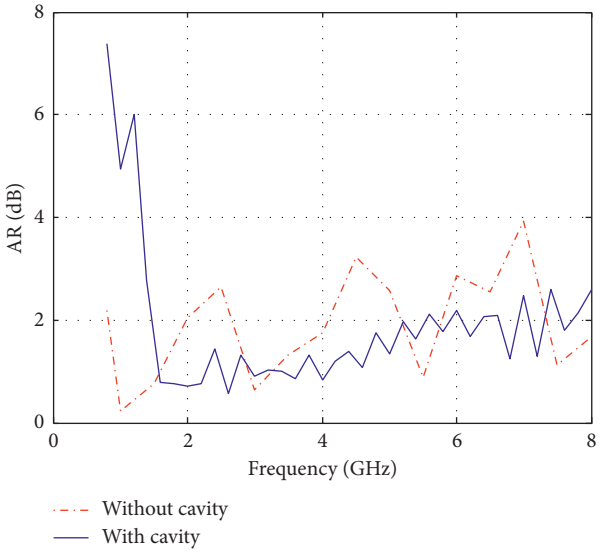

Figure 17: Simulated ARs of the SAAS antennas with and without a cavity.

has little influence on VSWR in the low-frequency band and makes no difference in the high-frequency band. Moreover, it exhibits good agreement with the simulated results.

The measured normalized radiation patterns of the SAAS antenna with metallic cavity and without metallic cavity are exhibited in Figure 23. It can be seen that the radiation is bidirectional without the metallic cavity. After the metallic cavity is employed, the radiation became unidirectional. The main polarization (right-handed circular polarization, RHCP) is approximately 10 dB higher than the cross polarization (left-handed circular polarization, LHCP). The measured results are in good agreement with the simulated results. The measured 3 dB beam width of the SAAS antenna at different frequencies is as follows: it is 108° at 1 GHz, 54° at 4 GHz, and 65°at 8 GHz. It also can be seen in

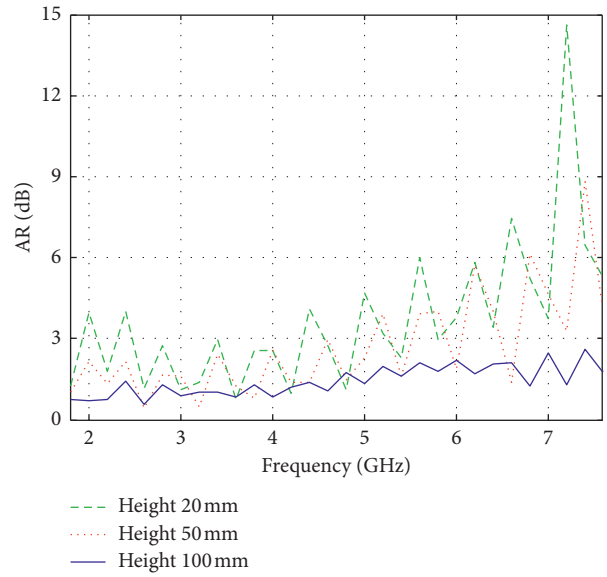

Figure 18: Simulated ARs of the SAAS antennas with different heights of cavity.

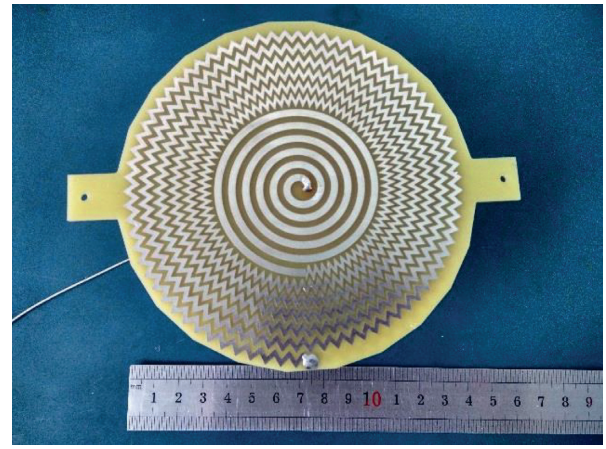

Figure 19: Prototype of the SAAS antenna.

Figure 23 that the maximum radiation direction changes with frequency. The antenna is designed for pantograph arcing detection in high-speed railways. Generally, the direction of the interference caused by pantograph arcing is unknown and random. In this case, an omnidirectional radiation pattern is preferred. However, the bandwidth of the omnidirectional antenna is usually narrow. Thus, the SAAS antenna is a good candidate for pantograph arcing detection, although its maximum radiation direction changes with frequency.

The measured and simulated gains of the SAAS antenna with metallic cavity are exhibited in Figure 24. It is seen that the measured antenna is not very high, which is below 3 dBi. The SAAS antenna is a bidirectional radiating antenna. The radiated electromagnetic waves towards the metallic back cavity are absorbed by the absorbing material that affects the antenna gain. However, the absorbing material is necessary for improving the S_{11} performance in the lower frequency

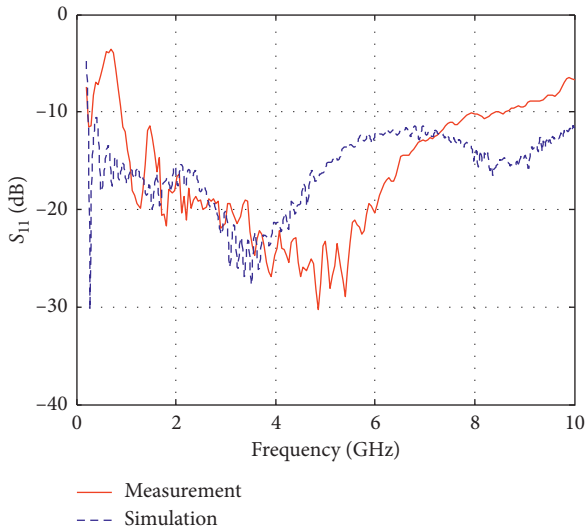

Figure 20: Measured and simulated reflection coefficient S_{11} of the antenna prototype.

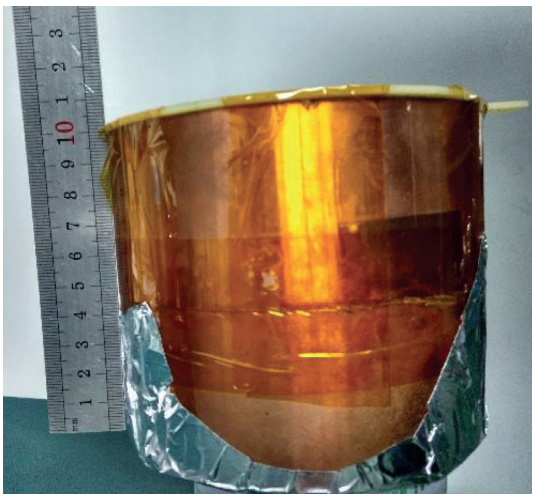

Figure 21: Prototype of the SAAS antenna with a back cavity.

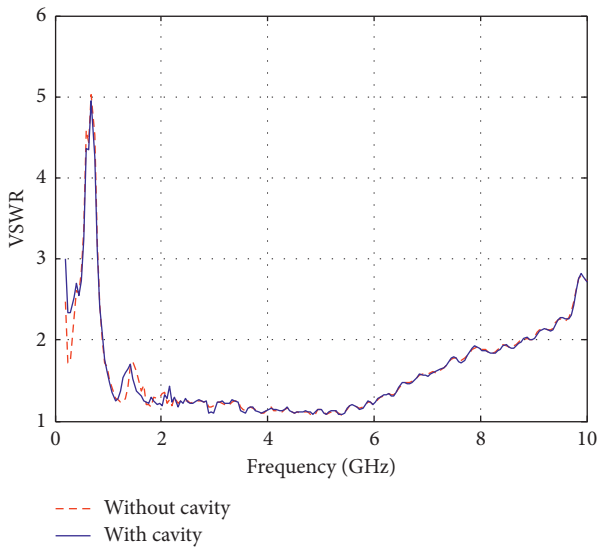

Figure 22: Measured VSWR of the antenna prototypes with and without back cavities.

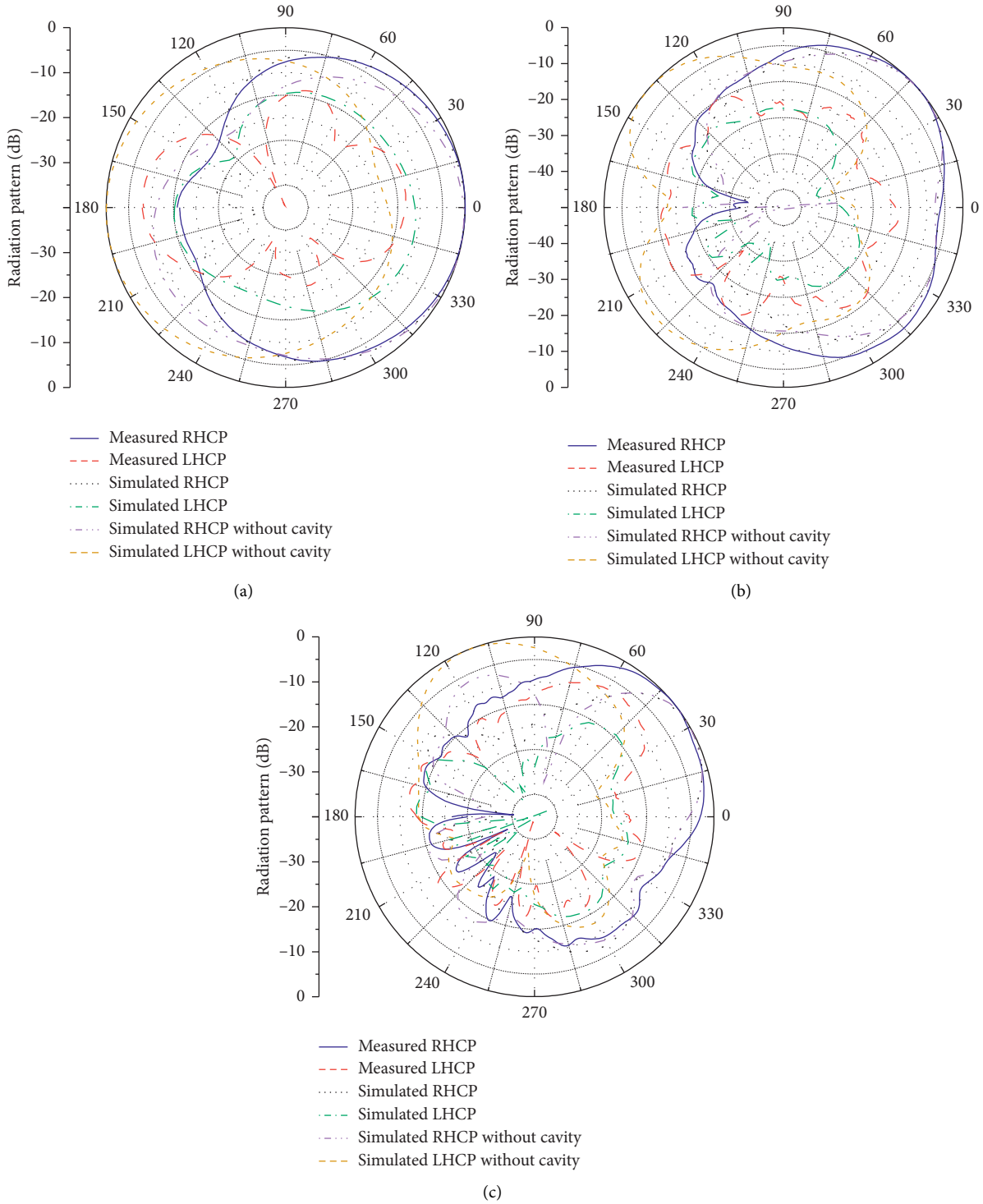

Figure 23: Measured and simulated normalized radiation patterns at different frequencies. (a) 1 GHz. (b) 4 GHz. (c) 8 GHz.

band. We make a trade-off between the antenna gain and the S_{11} performance. It is also seen in Figure 24 that the measured and simulated antenna gain has the same trend as frequency varying. The measured result is lower than the simulated result. This may be caused by the loss of the substrate which is not considered in the antenna simulation.

The measured and simulated ARs at different frequencies are illustrated in Figure 25. The simulated result of the AR without metallic cavity is below 3 dB from 1.2 GHz to 8 GHz, which is better than that with metallic cavity, especially at lower frequencies. It may be attributed to the metallic cavity under the substrate. Due to longer wavelengths at lower

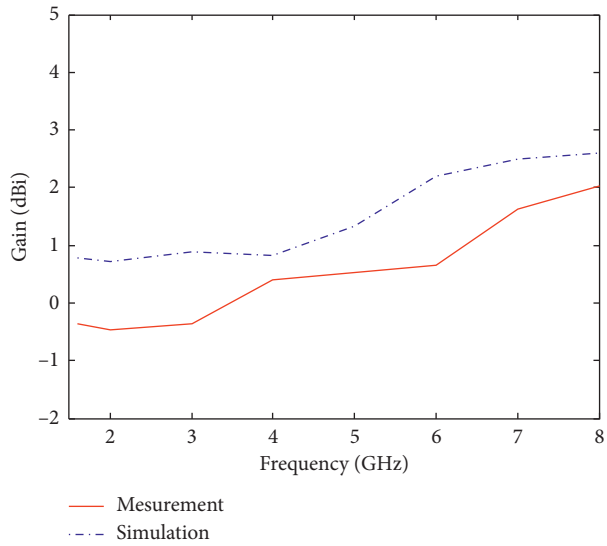

Figure 24: The simulated and measured gain of the SAAS antenna with a metallic cavity.

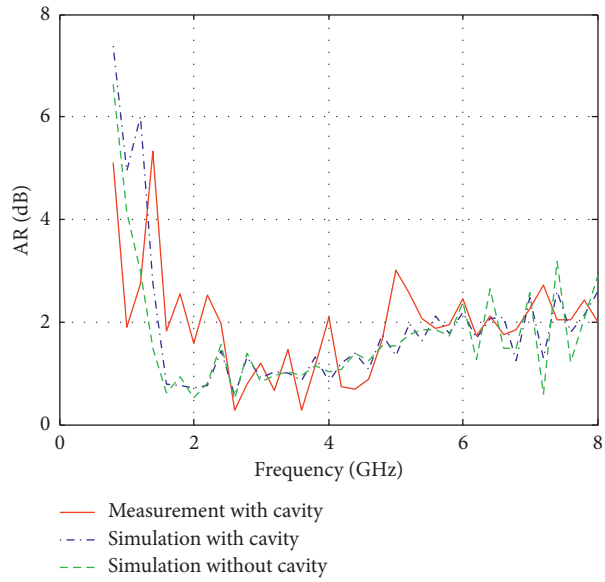

Figure 25: Measured ARs at different frequencies.

frequencies, the current distributions on antenna arms are more susceptible to be influenced by the metallic cavity, which leads to degraded AR performance. The measured AR with a cavity is less than 3 dB from 1.6 GHz to 8 GHz; that is, the AR bandwidth is 1 : 5. The measured AR is not as good as simulated AR in lower frequencies, which may be caused by the nonideal absorbing material.

The measured ARs at different angles are shown in Figure 26. We can see that the measured ARs are below 3 dB from -50° to 50° as the frequency below 5 GHz. The ARs are approximate below 3 dB from -20° to 20° as the frequency above 6 GHz. This degradation is related to the disc ground. The disc ground acts as a reflector, which will cause distortion of the current on the antenna arm. When the working frequency increases, the active radiating area concentrates towards the antenna center. Thus, the AR performances at higher frequencies are more susceptible to be influenced by the disc ground.

We make a comparison between the proposed antenna and antennas in other literature. Compared with the single-arm spiral antennas in other references, the proposed antenna has a wider impedance bandwidth 1 : 10.0 and AR bandwidth 1 : 5.0, as reported in Table 1. However, the cavity height of the proposed antenna is $0.29\lambda_L$ which is not as good as that in other literature. Because traditional metallic cavity is employed in our antenna design, technology that is beneficial to reduce the cavity height should be considered to decrease the antenna profile in the future.

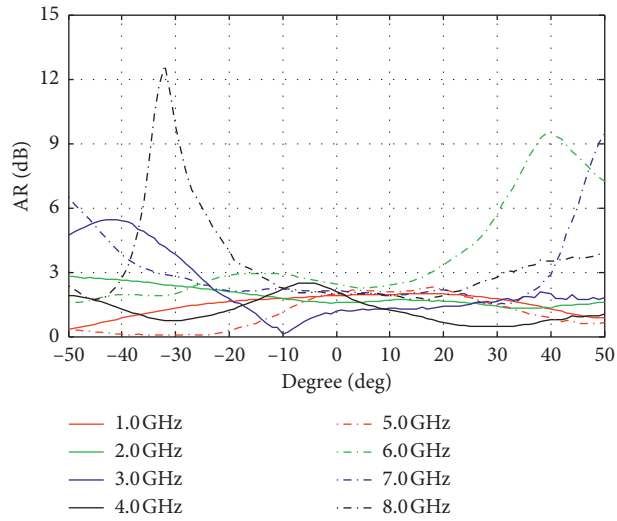

Figure 26: The ARs at different angles.

Table 1: Comparisons between spiral antennas in different studies.

Literature	Antenna circumference	Cavity height	Impedance bandwidth	AR bandwidth
[5]	$0.84\lambda_L$	$0.13\lambda_L$	1 : 5.4	1 : 4.8
[12]	$2.14\lambda_L$	$0.07\lambda_L$	1 : 3.3	1 : 3.3
[14]	$0.83\lambda_L$	$0.07\lambda_L$	1 : 3.0	1 : 3.0
[23]	$1.57\lambda_L$	$0.13\lambda_L$	1 : 2.5	—
[24]	$1.12\lambda_L$	No cavity	1 : 2.3	1 : 1.6
[25]	$1.43\lambda_L$	$0.12\lambda_L$	1 : 4.4	1 : 3.0
Ours	$1.27\lambda_L$	$0.29\lambda_L$	1 : 10.0	1 : 5.0

5. Conclusions

An SAAS antenna is proposed and studied in this paper. The performance of the proposed antenna, including the reflection coefficient, input impedance, current distribution, radiation pattern, and AR, are studied. It is illustrated that the meandered arm structure is effective in improving the circular polarization at low-frequency. Moreover, it is also an effective way to reduce the antenna size. With a metallic cavity, the proposed antenna can realize unidirectional radiation. The measurement results indicate that the proposed SAAS antenna can realize a wide AR bandwidth of 1 : 5.

Data Availability

The data that support the findings of this study are available from the corresponding author upon reasonable request.

Conflicts of Interest

The authors declare that there are no conflicts of interest regarding the publication of this study.

Acknowledgments

This work was supported by the Natural Science Foundation of China (Grant nos. 61801309 and 51807123), the Natural Science Foundation of Hebei Province (Grant no. F2018210136), and the Postdoctoral Science Foundation (Grant no. 2017M623400).

References

[1] Y. Han, H. Wang, Z. Wang et al., "Dual-band spiral printed quadrifilar helical antenna miniaturized by surface and inner dielectric loading," *IEEE Access*, vol. 7, pp. 30244–30251, 2019.

[2] R. N. Pack, G. Lasser, and D. S. Filipovic, "Performance characterization of four-arm MAW spiral antennas for digital direction-of-arrival sensing," *IEEE Transactions on Antennas and Propagation*, vol. 66, no. 6, pp. 2761–2769, 2018.

[3] H. Nakano, K. Nogami, S. Arai et al., "A spiral antenna backed by a conducting plane reflector," *IEEE Transactions on Antennas and Propagation*, vol. 34, no. 6, pp. 791–796, 1986.

[4] Y. Yao, F. Zhang, and F. Zhang, "A new approach to design circularly polarized beam-steering antenna arrays without phase shift circuits," *IEEE Transactions on Antennas and Propagation*, vol. 66, no. 5, pp. 2354–2364, 2018.

[5] S. M. H. Ranjbaran and S. Mohanna, "Improved spiral antenna with a new semi-fractal reflector for short-range sensing," *IET Microwaves, Antennas & Propagation*, vol. 12, no. 11, pp. 1839–1845, 2018.

[6] Y. Zhong, G. Yang, J. Mo et al., "Compact circularly polarized Archimedean spiral antenna for ultrawideband communication applications," *IEEE Antennas and Wireless Propagation Letters*, vol. 16, pp. 129–132, 2016.

[7] C. Liu, Y. Lu, C. Jingbo, and X. Shen, "The broadband spiral antenna design based on hybrid backed-cavity," *IEEE Transactions on Antennas and Propagation*, vol. 58, no. 6, pp. 1876–1882, 2010.

[8] P. H. Rao, S. Sujitha, and K. T. Selvan, "A multiband, mutipolarization shared-aperture antenna: design and evaluation," *IEEE Antennas and Propagation Magazine*, vol. 59, no. 4, pp. 26–37, 2017.

[9] M. Ur-Rehman, G. A. Safdar, X. Yang et al., "Design and study of a circular polarised conical-disc-backed spiral antenna for X-band Applications," *IEEE Access*, vol. 5, pp. 21344–21354, 2017.

[10] H. Nakano, J. Miyake, T. Sakurada et al., "Dual-band counter circularly polarized radiation from a single-arm metamaterial-based spiral antenna," *IEEE Transactions on Antennas and Propagation*, vol. 61, no. 6, pp. 2938–2947, 2013.

[11] H. Nakano, T. Igarashi, H. Oyanagi et al., "Unbalanced-mode spiral antenna backed by an extremely shallow cavity," *IEEE Transactions on Antennas and Propagation*, vol. 57, no. 6, pp. 1625–1633, 2009.

[12] H. Nakano, R. Satake, and J. Yamauchi, "Extremely low-profile, single-arm, wideband spiral antenna radiating a circularly polarized wave," *IEEE Transactions on Antennas and Propagation*, vol. 58, pp. 1511–1520, 2010.

[13] H. Nakano, J. Eto, Y. Okabe et al., "Tilted- and axial-beam formation by a single-arm rectangular spiral antenna with compact dielectric substrate and conducting plane," *IEEE Transactions on Antennas and Propagation*, vol. 50, no. 5, pp. 17–24, 2002.

[14] Y. Oh and S. Nam, "Design of a low-profile 2 to 6 GHz circular polarized single arm hexagonal spiral array antenna," in *Proceedings of 2017 Applied Computational Electromagnetics Society Symposium (ACES)*, pp. 1-2, Firenze, Italy, March 2017.

[15] R. Rong-Lin Li and H. Nakano, "Numerical analysis of arbitrarily shaped probe-excited single-arm printed wire antennas," *IEEE Transactions on Antennas and Propagation*, vol. 46, no. 9, pp. 1307–1317, 1998.

[16] S. Jacobsen, H. O. Rolfsnes, and P. R. Stauffer, "Characteristics of microstrip muscle-loaded single-arm archimedean spiral antennas as investigated by FDTD numerical computations," *IEEE Transactions on Biomedical Engineering*, vol. 52, no. 2, pp. 321–330, 2005.

[17] Z. Zhang and G. Fu, "Broadband circularly polarized spiral antenna array," in *Proceedings of 2015 IEEE 4th Asia-Pacific Conference on Antennas and Propagation (APCAP)*, pp. 582–584, Bali Island, Indonesia, June 2015.

[18] A. Mehta, D. Mirshekar-Syahkal, and H. Nakano, "Beam adaptive single arm rectangular spiral antenna with switches," *IEEE Proceedings-Microwaves, Antennas and Propagation*, vol. 153, no. 1, pp. 13–18, 2006.

[19] C. Jung, M. Lee, G. P. Li et al., "Reconfigurable scan-beam single-arm spiral antenna integrated with RF-MEMS switches," *IEEE Transactions on Antennas and Propagation*, vol. 54, no. 2, pp. 455–463, 2006.

[20] P. Deo, A. Mehta, D. Mirshekar-Syahkal et al., "An HIS-based spiral antenna for pattern reconfigurable applications," *IEEE Antennas and Wireless Propagation Letters*, vol. 8, pp. 196–199, 2009.

[21] C. Sharma and D. K. Vishwakarma, "Miniaturization of spiral antenna based on fibonacci sequence using modified koch curve," *IEEE Antennas and Wireless Propagation Letters*, vol. 16, no. 99, pp. 932–935, 2017.

[22] H. Xu, G. Wang, and T. Cai, "Miniaturization of 3-D anistropic zero-refractive-index metamaterials with application to directive emissions," *IEEE Transactions on Antennas and Propagation*, vol. 62, no. 6, pp. 3141–3149, 2014.

[23] J. Ahn, S. H. Cha, S. G. Cha et al., "Compact spiral element for wideband beam-steering arrays," *IEEE Antennas and Wireless Propagation Letters*, vol. 16, pp. 1994–1997, 2017.

[24] O. Ahmad Mashaal, S. K. A. Rahim, A. Y. Abdulrahman et al., "A coplanar waveguide fed two arm archimedean spiral slot antenna with improved bandwidth," *IEEE Transactions on Antennas and Propagation*, vol. 61, no. 2, pp. 939–943, 2013.

[25] Y. Zhong, G. Yang, J. Mo et al., "Compact circularly polarized archimedean spiral antenna for ultrawideband communication applications," *IEEE Antennas and Wireless Propagation Letters*, vol. 16, pp. 129–132, 2017.